

# Importance of Fermi surface and magnetic interactions for the superconducting dome in electron doped FeSe intercalates

## – Supplemental Material –

Makoto Shimizu,<sup>1</sup> Nayuta Takemori,<sup>2</sup> Daniel Guterding,<sup>3</sup> and Harald O. Jeschke<sup>2</sup>

<sup>1</sup>*Department of Physics, Okayama University, Okayama 700-8530, Japan*

<sup>2</sup>*Research Institute for Interdisciplinary Science, Okayama University, Okayama 700-8530, Japan*

<sup>3</sup>*Fachbereich Mathematik, Naturwissenschaften und Datenverarbeitung,*

*Technische Hochschule Mittelhessen, Wilhelm-Leuschner-Straße 13, 61169 Friedberg, Germany*

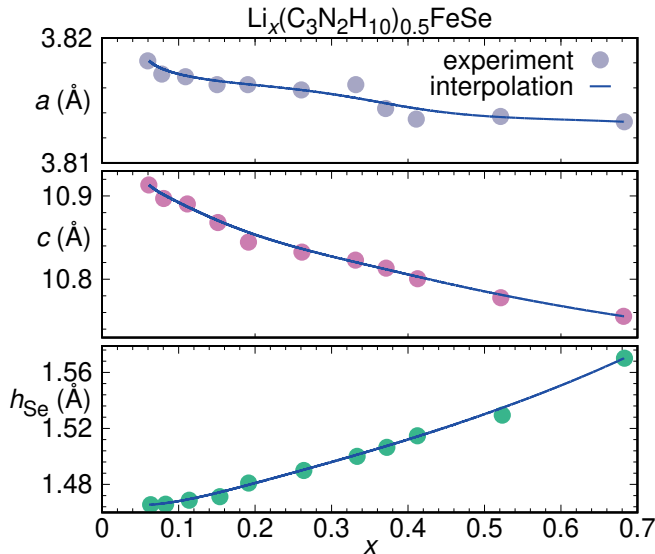


FIG. S1. Structural parameters from Ref. 1 (symbols) and interpolation (lines). Calculations were performed for interpolated structures in steps of  $\Delta x = 0.01$ .

### I. CRYSTAL STRUCTURES

The study of  $\text{Li}_x(\text{C}_3\text{N}_2\text{H}_{10})_{0.37}\text{FeSe}$  requires preparation of model structures as the experimental crystal structure provided in Ref. 1 contains some disorder and is not directly amenable to DFT calculations. First of all, the diaminopropane molecule is placed on an  $8g$  Wyckoff position of the  $P4_21_2$  space group with partial occupancy of 0.093, leading to 0.372  $\text{C}_3\text{N}_2\text{H}_{10}$  molecules per FeSe. We simplify this structure by lowering the symmetry to  $P1$  and by picking one of the eight symmetry equivalent  $\text{C}_3\text{N}_2\text{H}_{10}$  molecules. This leads to the approximate stoichiometry  $\text{Li}_x(\text{C}_3\text{N}_2\text{H}_{10})_{0.5}\text{FeSe}$ . This structure is shown in Figure 1 of the main text. Note that Sun *et al.* show a very similar simplified structure<sup>1</sup>. The simplification is justified because the diaminopropane molecules are important for fixing the interlayer distance; however, electronically, the highest occupied molecular orbitals are significantly below the Fermi level while the lowest unoccupied molecular orbital is slightly above the Fermi level so that the molecules are not active at the Fermi level. In order to obtain a finely spaced series of crystal

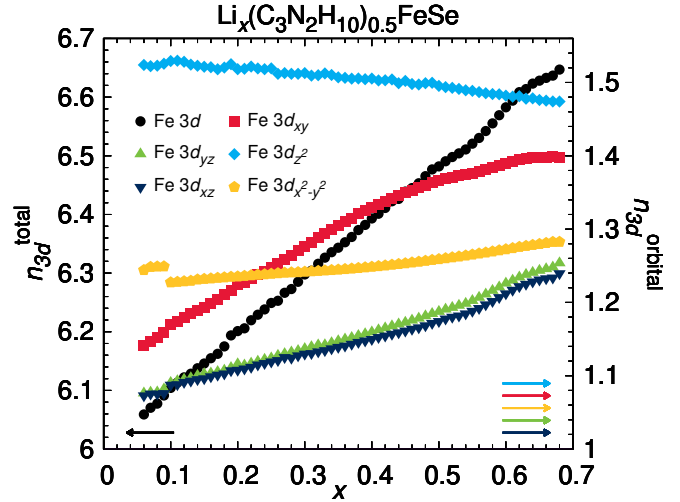


FIG. S2. Evolution of the total and orbital resolved Fe  $3d$  occupation number as a function of doping.

structures of  $\text{Li}_x(\text{C}_3\text{N}_2\text{H}_{10})_{0.5}\text{FeSe}$  as a function of doping level  $x$ , we interpolate the structural data provided in Ref. 1 as shown in Figure S1. This guarantees that we do not incur the well-known difficulties of predicting the chalcogenide  $z$  position in iron chalcogenide superconductors. Combining the diaminopropane molecule coordinates given for  $x = 0.26$  with the lattice parameters of Figure S1 would lead to expanded or compressed molecules as a function of doping. This would be unrealistic as the molecules remain approximately neutral over the whole doping range, and their bonds should be rigid. Therefore, we adapt the diaminopropane molecule Wyckoff positions to the changing lattice parameters, keeping all distances and angles within the molecules constant. We model the doping  $x$  by using the virtual crystal approximation for Li, using a nuclear charge between neon and lithium of  $Z = 2 + x$ .

### II. ELECTRONIC PROPERTIES

In Figure S3, we show the unfolded one iron Fermi surfaces of  $\text{Li}_x\text{FeSe}$  with  $\text{C}_3\text{N}_2\text{H}_{10}$  molecules for six doping levels. The corresponding Fermi surfaces of  $\text{Li}_x(\text{C}_3\text{N}_2\text{H}_{10})_{0.5}\text{FeSe}$  are shown in the main

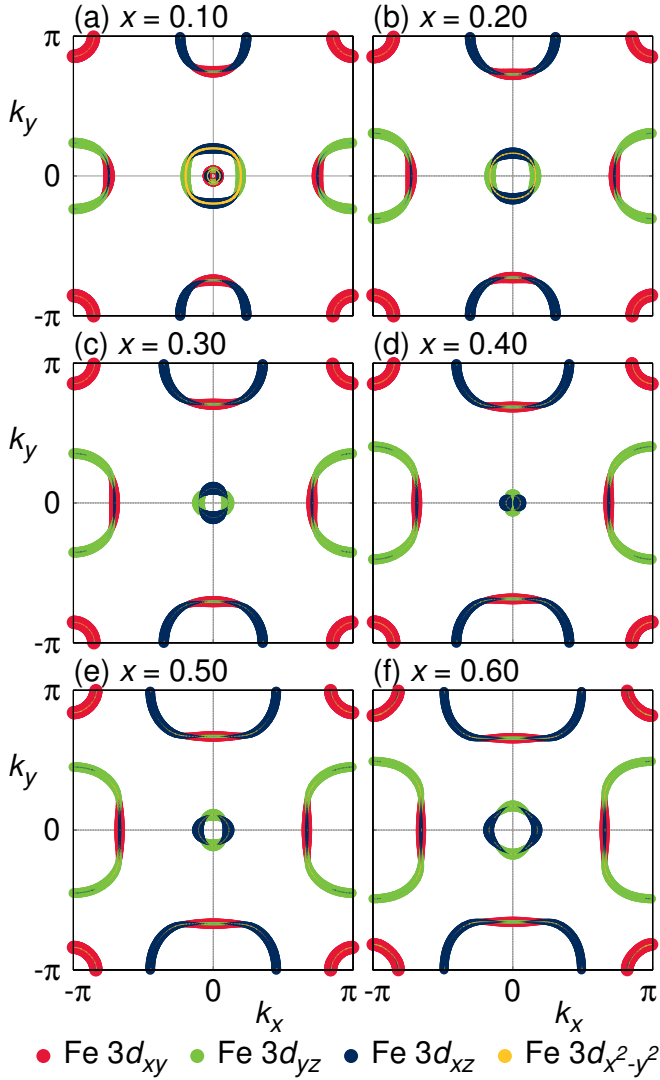


FIG. S3. Evolution of the Fermi surface at  $k_z = 0$  with doping for  $\text{Li}_x\text{FeSe}$  without  $\text{C}_3\text{N}_2\text{H}_{10}$  molecule. The Fe 3d orbital weights are indicated by color. Orbital weight of Fe  $3d_{z^2}$  at the Fermi level is nearly negligible.

text. In Figure S2, we show electron densities of  $\text{Li}_x(\text{C}_3\text{N}_2\text{H}_{10})_{0.5}\text{FeSe}$  as a function of doping levels  $0.06 \leq x \leq 0.68$ . The data are obtained by integrating iron total and orbital resolved densities of states up to the Fermi level.

Figure S4 shows the density of states at the Fermi level  $N(E_F)$  with and without  $\text{C}_3\text{N}_2\text{H}_{10}$  molecule.  $N(E_F)$  of the ten-band tight binding model faithfully represents the DFT result. On the other hand, there is some deviation for the unfolded five-band tight binding model for larger dopings, and in particular in the range  $0.55 < x < 0.62$  as discussed in the main text. These deviations stem from the dopants, which lower the crystal symmetry compared to pristine FeSe, so that the unfolding to the five band model becomes only approximate.

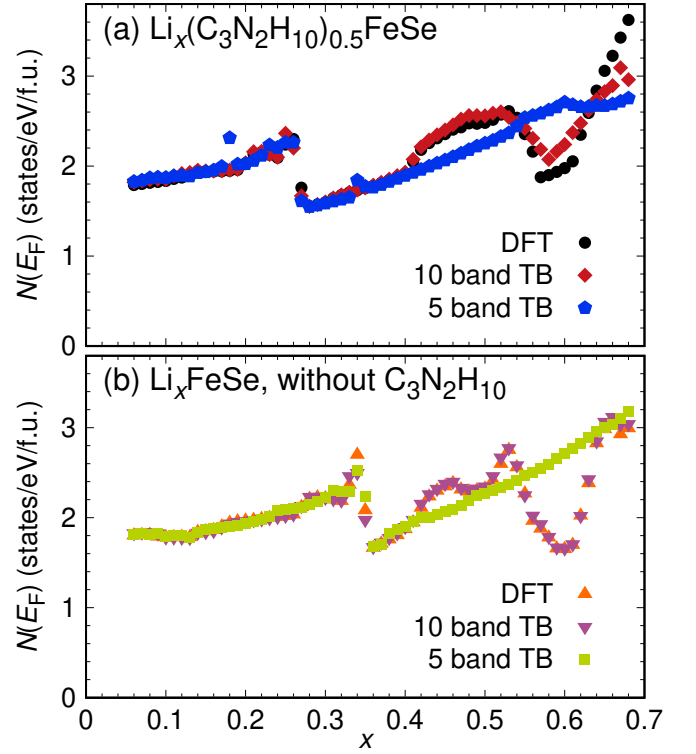


FIG. S4. Density of states at the Fermi level  $N(E_F)$  for the two series of structures used in this study. (a) Full structure with diaminopropane molecule, (b)  $\text{Li}_x\text{FeSe}$  with empty van der Waals gap.

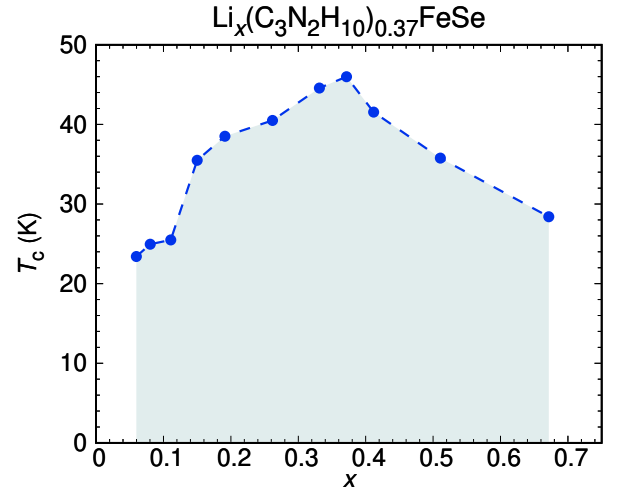


FIG. S5. Superconducting  $T_c$  of  $\text{Li}_x(\text{C}_3\text{N}_2\text{H}_{10})_{0.5}\text{FeSe}$  as a function of doping, as reported in Ref. 1.

### III. ENERGY MAPPING

The exchange couplings of  $\text{Li}_x(\text{C}_3\text{N}_2\text{H}_{10})_{0.5}\text{FeSe}$  were determined by the energy mapping technique<sup>2,3</sup>. They are listed in Table S1.  $2 \times 2 \times 1$  supercells with  $P1$  symmetry contain eight inequivalent iron sites, allowing for 13 spin configurations with different energies. Two exam-

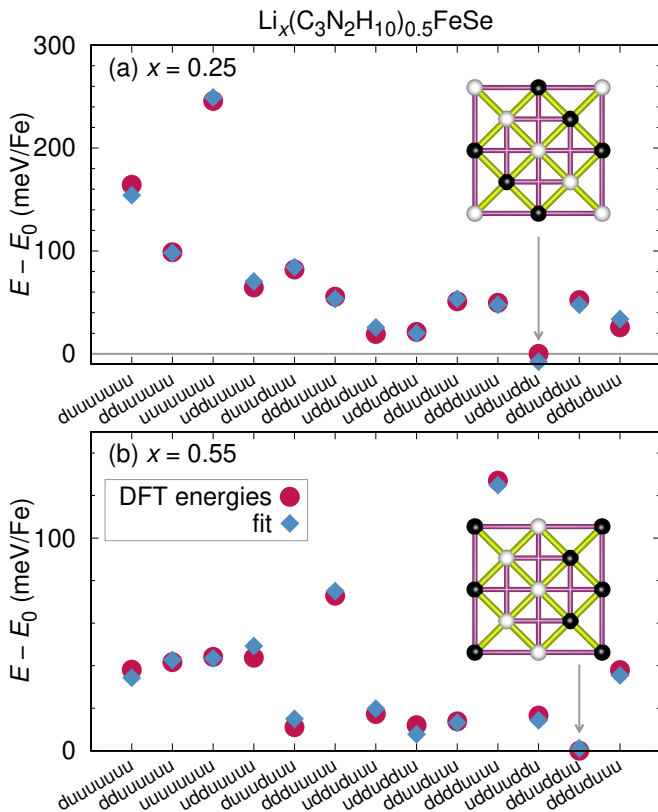


FIG. S6. Two examples for the energy mapping of  $\text{Li}_x(\text{C}_3\text{N}_2\text{H}_{10})_{0.5}\text{FeSe}$  at (a)  $x = 0.25$  and (b)  $x = 0.55$ . In both panels the inset shows an eight iron supercell with the minimum energy spin configuration marked by white for up and black for down. Up to a doping of  $x = 0.45$ , the stripe-type order is lowest in energy, while from  $x = 0.5$ , the bicollinear order is stabilized.

ples are shown in Figure S6. Due to the metallic nature of the FeSe intercalate, the fit to the DFT energies is not as good as in magnetic insulators<sup>4</sup> but it is very reasonable as indicated by the small deviations between fitted and DFT energies and by the small error bars shown in Figure 5 of the main text. Note that at large doping, the bicollinear configuration takes over from stripe-type as lowest energy spin configuration (Figure S6).

#### IV. ITERATIVE MINIMIZATION METHOD

The iterative minimization method allows the efficient determination of ground state spin configurations of classical spin systems<sup>5,6</sup>. We use this method to obtain the ground states of the classical Heisenberg models with the exchange couplings in Table S1. We Fourier transform the obtained spin configurations to obtain the spin structure factor  $S(\mathbf{q})$ . The spin structure factors of  $\text{Li}_x(\text{C}_3\text{N}_2\text{H}_{10})_{0.5}\text{FeSe}$  for doping values  $x = 0.10$  and  $x = 0.60$  are shown in Fig. S7. In the doping region of  $0.10 \leq x \leq 0.45$ , we find peaks at  $\mathbf{q} = (\pi, 0)$  or  $\mathbf{q} = (0, \pi)$ ,

TABLE S1. Exchange couplings of  $\text{Li}_x(\text{C}_3\text{N}_2\text{H}_{10})_{0.5}\text{FeSe}$ , calculated with GGA and  $4 \times 4 \times 4$   $k$  points. The errors shown are only the statistical error arising from the energy mapping.

$x$	$J_1$ (meV)	$J_2$ (meV)	$J_3$ (meV)
0.1	72.3(2.7)	44.1(2.2)	4.5(2.0)
0.15	66.7(2.2)	43.4(1.8)	4.8(1.7)
0.2	59.7(2.1)	41.5(1.7)	5.1(1.6)
0.25	50.4(2.0)	39.0(1.6)	5.7(1.5)
0.3	39.5(1.9)	35.9(1.6)	6.6(1.5)
0.35	28.4(1.7)	33.0(1.4)	7.6(1.3)
0.4	16.9(1.4)	29.6(1.1)	8.8(1.0)
0.45	4.9(1.1)	25.7(9)	10.3(8)
0.5	-7.3(1.0)	21.6(8)	11.2(8)
0.55	-20.4(1.1)	17.5(9)	12.0(9)
0.6	-33.1(1.1)	13.0(9)	12.2(8)

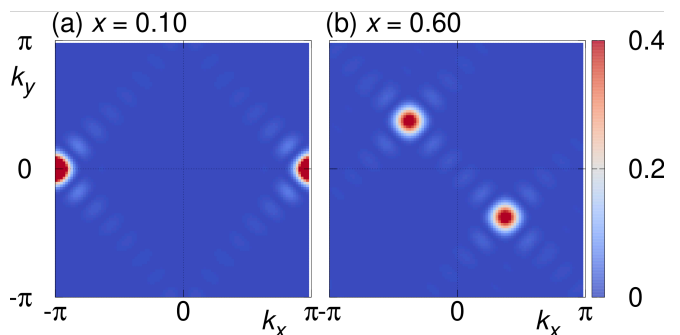


FIG. S7. Spin structure factors  $S(\mathbf{q})$  at  $x = 0.10$  and  $x = 0.60$ , obtained by Fourier transforming the ground state spin configuration found with iterative minimization.

indicating stripe AFM order as ground states. On the other hand, for  $0.50 \leq x \leq 0.60$ , as soon as  $J_1$  turns ferromagnetic, we find peaks at  $\mathbf{Q} = (q, q)$  where  $q \sim 0.4\pi$ . As it is well known that FeSe also has a substantial bi-quadratic coupling<sup>7</sup> which we do not re-determine here, the highly doped  $\text{Li}_x(\text{C}_3\text{N}_2\text{H}_{10})_{0.5}\text{FeSe}$  samples will actually be in the bicollinear phase with  $\mathbf{q} = (\pi/2, \pi/2)$  and magnetically resemble FeTe.

<sup>1</sup> R. J. Sun, Y. Quan, S. F. Jin, Q. Z. Huang, H. Wu, L. Zhao, L. Gu, Z. P. Yin, and X. L. Chen, Realization of continuous

electron doping in bulk iron selenides and identification of a

- new superconducting zone, *Phys. Rev. B* **98**, 214508 (2018).
- <sup>2</sup> H. O. Jeschke, I. Opahle, H. Kandpal, R. Valentí, H. Das, T. Saha-Dasgupta, O. Janson, H. Rosner, A. Brühl, B. Wolf, M. Lang, J. Richter, S. Hu, X. Wang, R. Peters, T. Pruschke, and A. Honecker, Multi-step approach to microscopic models for frustrated quantum magnets: The case of the natural mineral azurite, *Phys. Rev. Lett.* **106**, 217201 (2011).
- <sup>3</sup> H. O. Jeschke, H. Nakano, and T. Sakai, From kagome strip to kagome lattice: Realizations of frustrated  $S = 1/2$  antiferromagnets in Ti(III) fluorides, *Phys. Rev. B* **99**, 140410 (2019).
- <sup>4</sup> Y. Iqbal, T. Müller, K. Riedl, J. Reuther, S. Rachel, R. Valentí, M. J. P. Gingras, R. Thomale, H. O. Jeschke, Signatures of a gearwheel quantum spin liquid in a spin- $1/2$  pyrochlore molybdate Heisenberg antiferromagnet, *Phys. Rev. Mater.* **1**, 071201(R) (2017).
- <sup>5</sup> M. F. Lapa and C. L. Henley, Ground States of the Classical Antiferromagnet on the Pyrochlore Lattice, arXiv:1210.6810.
- <sup>6</sup> Y. Iqbal, T. Müller, H. O. Jeschke, R. Thomale, and J. Reuther, Stability of the spiral spin liquid in  $\text{MnSc}_2\text{S}_4$  *Phys. Rev. B* **98**, 064427 (2018).
- <sup>7</sup> J. K. Glasbrenner, I. I. Mazin, H. O. Jeschke, P. J. Hirschfeld, R.M. Fernandes, and R. Valentí, Effect of magnetic frustration on nematicity and superconductivity in iron chalcogenides, *Nat. Phys.* **11**, 953 (2015).